

# DARK MATTER CONSTRAINTS FROM AN OBSERVATION OF DSPHS AND THE LMC WITH THE BAIKAL NT200

*A. D. Avrorin*<sup>a</sup>, *A. V. Avrorin*<sup>a</sup>, *V. M. Aynutdinov*<sup>a</sup>, *R. Bannasch*<sup>i</sup>, *I. A. Belolaptikov*<sup>b</sup>,  
*V. B. Brudanin*<sup>b</sup>, *N. M. Budnev*<sup>c</sup>, *I. A. Danilchenko*<sup>a</sup>, *S. V. Demidov*<sup>a\*</sup>,  
*G. V. Domogatsky*<sup>a</sup>, *A. A. Doroshenko*<sup>a</sup>, *R. Dvornicky*<sup>b,g</sup>, *A. N. Dyachok*<sup>c</sup>,  
*Zh.-A. M. Dzhilkibaev*<sup>a</sup>, *L. Fajt*<sup>g,h</sup>, *S. V. Fialkovsky*<sup>e</sup>, *A. R. Gafarov*<sup>c</sup>, *O. N. Gaponenko*<sup>a</sup>,  
*K. V. Golubkov*<sup>a</sup>, *T. I. Gress*<sup>c</sup>, *Z. Honz*<sup>b</sup>, *K. G. Kebkal*<sup>i</sup>, *O. G. Kebkal*<sup>i</sup>, *K. V. Konischev*<sup>b</sup>,  
*A. V. Korobchenko*<sup>c</sup>, *A. P. Koshechkin*<sup>a</sup>, *F. K. Koshel*<sup>a</sup>, *A. V. Kozhin*<sup>d</sup>, *V. F. Kulepov*<sup>e</sup>,  
*D. A. Kuleshov*<sup>a</sup>, *M. B. Milenin*<sup>e</sup>, *R. A. Mirgazov*<sup>c</sup>, *E. R. Osipova*<sup>d</sup>, *A. I. Panfilov*<sup>a</sup>,  
*L. V. Pan'kov*<sup>c</sup>, *E. N. Pliskovsky*<sup>b</sup>, *M. I. Rozanov*<sup>f</sup>, *E. V. Rjabov*<sup>c</sup>, *B. A. Shaybonov*<sup>b</sup>,  
*A. A. Sheifler*<sup>a</sup>, *M. D. Shelepov*<sup>a</sup>, *A. V. Skurihin*<sup>d</sup>, *O. V. Suvorova*<sup>a\*\*</sup>, *V. A. Tabolenko*<sup>c</sup>,  
*B. A. Tarashansky*<sup>c</sup>, *S. A. Yakovlev*<sup>i</sup>, *A. V. Zagorodnikov*<sup>c</sup>, *V. L. Zurbanov*<sup>c</sup>

<sup>a</sup> *Institute for Nuclear Research RAS, 117312 Moscow, Russia*

<sup>b</sup> *Joint Institute for Nuclear Research, Dubna, Russia*

<sup>c</sup> *Irkutsk State University, Irkutsk, Russia*

<sup>d</sup> *Skobeltsyn Institute of Nuclear Physics MSU, Moscow, Russia*

<sup>e</sup> *Nizhni Novgorod State Technical University, Nizhni Novgorod, Russia*

<sup>f</sup> *St.Petersburg State Marine University, St.Petersburg, Russia*

<sup>g</sup> *Comenius University, Mlynská dolina F1, SK-842 48 Bratislava, Slovakia*

<sup>h</sup> *Czech Technical University in Prague, 12800 Prague, Czech Republic*

<sup>i</sup> *EvoLogics GmbH, Berlin, Germany*

In present analysis we complete search for a dark matter signal with the Baikal neutrino telescope NT200 from potential sources in the sky. We use five years of data and look for neutrinos from dark matter annihilations in the dwarfs spheroidal galaxies in the Southern hemisphere and the Large Magellanic Cloud known as the largest and close satellite galaxy of the Milky Way. We do not find any excess in observed data over expected background from the atmospheric neutrinos towards the LMC or any of tested 22 dwarfs. We perform a joint likelihood analysis on the sample of five selected dwarfs and found a concordance of the data with null hypothesis of the background-only observation. We derive 90% CL upper limits on the cross section of annihilating dark matter particles of mass between 30 GeV and 10 TeV into several channels both in our combined analysis of the dwarfs and in a particular analysis towards the LMC.

\* E-mail: demidov@ms2.inr.ac.ru

\*\* E-mail: suvorova@cpc.inr.ac.ru

## 1. INTRODUCTION

Vast majority of astrophysical and cosmological observational data indicate on existence of new particles – dark matter (DM) [1]. The natural and the most favorable candidate for this phenomena is Weakly Interacting Massive Particles (WIMP) [2]. Their main property is possibility of annihilation into pairs of ordinary matter particles followed by their decays and hadronization. Searches for such annihilation signal from different astrophysical objects are performed by numerous experiments including neutrino telescopes.

The dwarf spheroidal galaxies (dSphs) being distant satellites of the Milky Way (MW) are optically faint or ultra-faint astrophysical objects, with the visible angular sizes less than about degree appeared to an observer. The dwarfs are characterized by a very small light-to-mass ratios and the flat rotation curves (see e.g. Refs. [3] and references therein), that suggests considerable dark matter content. As a consequence, the dSphs are considered as sources of significant dark matter annihilation signal, while the experimental controversies are widely discussed (see e.g. Refs. [4–7]). Upto now about four dozens of dSphs have been discovered, with account of new eight dwarfs recently found by the DES [8,9]. Their visible population in the sky might be increased significantly due to new optical imaging surveys i.e. DES [10] and LSST [11] and complementary observations with the gamma-telescopes of a next generation like the CTA [12]. This will open new opportunities in the DM investigation. Presently, among many multimessenger searches for DM annihilation signal from extragalactic sources like the dSphs, there was not found significant excess in the number of events relatively to estimated background. Furthermore, there are robust upper bounds on the DM annihilation signal in the joint analysis of the dSphs obtained with the gamma-telescopes FERMI-LAT and DES [13–15], also the MAGIC [16] and the HESS [17]. Similar search of the indirect DM signal has been performed with the IceCube [18] and as well in the current work on base of the neutrinos detection. Evidence of dark matter repository in the nearby and the largest satellite galaxy of the Milky Way i.e. the Large Magellanic Cloud (LMC) makes this region by the second brightest astrophysical source of DM annihilations [19] after the MW Galactic Center (GC) [20,21]. The recent analysis of the FERMI-LAT data [22] shows that the obtained upper limits on the DM annihilation signal in the LMC are quite competitive with those from the dSphs, despite the LMC unlike the dwarfs has significant baryonic background.

High energy neutrinos incoming from the directions towards the dwarfs or the LMC are expected to be among the copious particles generated in the different DM annihilation channels. If these neutrinos have their energies above an energy threshold, they have probability to be detected by neutrino telescopes. A major challenge is to suppress background of the atmospheric muons exceeding upward going neutrino flux by the factor  $10^6$ . A particular aim is to resolve non-atmospheric origin of neutrinos towards the DM sources in a search for indirect signal of dark matter taking into account known uncertainties both experimental, theoretical and astrophysical.

In the present analysis we use the NT200 neutrino dataset, perform a search for an excess in the directions towards the LMC and dSphs and put constraints on dark matter annihilation cross section. The paper is organized as follows. In section 2 we shortly recall the experiment NT200 and the data selection. In section 3 we describe signal and background properties and their simulation for the the cases of dwarfs galaxies and the LMC. In section 4 we obtain upper limits on dark matter annihilation cross section and make a comparison with the results from other experiments. Conclusions are presented in section 5.

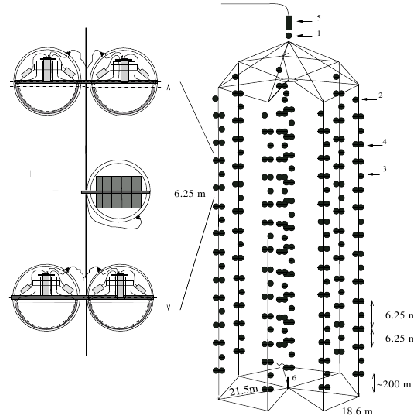


**Fig. 1.** NT200 schematic view: 1 – array electronics module; 2 – string electronics module; 3 – "svjaska" (shown on left separately) i.e. two pairs of OMs with electronics module; 4 – pair of OMs; 5 and 6 – calibration lasers.

## 2. EXPERIMENT AND OBSERVATION

In a search for dark matter signal, we use measured directions of muons arriving to the Baikal neutrino telescope NT200. This is indirect method to estimate a signal strength with subsequent off-line optimization of signal to background ratio. Cherenkov radiation of muons and hadronic showers induced by relativistic neutrino scatterings off nucleons in surrounding water is distinctive by fixed Cherenkov angle (about  $42^\circ$  in water) relatively the track of moving relativistic particle at each point of its path. It is a base in reconstruction of arrival time of particle and its angular coordinates. The Cherenkov emission is effectively collected by optical modules (OMs) in 3D-configuration of photodetectors on strings, while the efficiency of this detection is strongly determined by hydro-optically properties of medium (see e.g. Ref. [23] and references therein).

The telescope NT200 is placed at  $51.83^\circ$  North latitude in the southern basin of the lake Baikal, at a distance of 3.5 km off the shore and at a depth of 1.1 km, its instrumentation volume encloses 100 Ktons. The optical properties of the Baikal water are characterized by the absorption length  $20 \div 24$  m at 480 nm and the scattering length  $30 \div 70$  m depending on a season. Recall (see Fig. 1) that the detector NT200 consists of 192 optical modules arranged in pairwise at twelve storeys ("svjaska" is shown with zoom) on 8 strings of 72 m length: seven peripheral strings and a central one. The distances between the strings are about 21.5 m. They are placed at vertices of heptagon with side of 18.5 m of size. Each OM contains hybrid photodetector QUASAR-370, a photo multiplier tube (PMT) with 37-cm diameter. To suppress background from dark noise, the two PMTs of a pair are switched in coincidence within a time window of 15 ns. The OMs are time-synchronized and energy-calibrated by artificial light pulses. The operated configurations of the NT200, its functional systems and the calibration methods have been described elsewhere [24–27].

In present analysis of the Baikal NT200 survey of the sky we used dataset for five years between April of 1998 and February of 2003, with in total 2.76 live years. The same dataset and the same Monte Carlo (MC) sample has been implemented in our searches for a DM annihilation signal towards the Sun [28] and the Galactic Center [29]. In particular, we have used dataset selected by the off-line filter with requirements of at least 6 hits on at least 3 strings ("muon trigger 6/3"), that selects about 40% of all triggered events with angular resolution of about  $14.1^\circ$  in term of the r.m.s. mismatch angle  $\psi_{reco}$ . To get the best possible estimator for the direction, we use multiple start guesses for the  $\chi^2$  minimization [30]. Basic analysis on distinguish upward and downward going muons on a one-per-million mis-assignment level has been done earlier [31], where the code was developed

for the atmospheric neutrinos ( $\nu_{atm}$ ). Study of the NT200 response on the fluxes of atmospheric muons and neutrinos has been done with the MC simulations based on the standard codes CORSIKA [32] and MUM [33] using the Bartol atmospheric  $\nu$  flux [34]. For the final filter of events the quality parameters are applied and they are not related to the time information e.g. variables like the number of hit channels,  $\chi^2/d.o.f.$ , the probability of fired channels to have been hit and not fired channels haven't been hit and the actual position of the track with respect to the detector center (for more details see Ref. [30,31]). To suppress background muons which are downgoing near horizon we select only the events with the reconstructed zenith angle  $\Theta > 100^\circ$ . All the cuts provide rejection factor for the atmospheric muons of about  $10^{-7}$ . Selection by the quality criteria results in data sample of 510 events for current analysis, having the neutrino energy threshold of about 10 GeV and median value  $2.5^\circ$  in the mismatch angles distribution, as it is seen in Fig. 2. In MC simulations of signal events

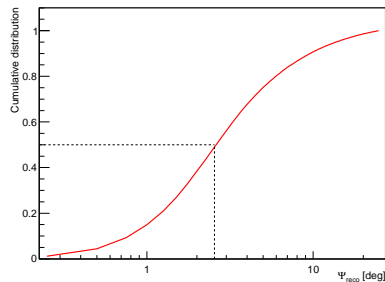


**Fig. 2.** The cumulative distribution of the mismatch angle  $\Psi_{reco}$  in the NT200 dataset reconstruction. The black-dotted line indicates the median value.

to be described in the next section we have applied the shape of differential  $\Psi_{reco}$  distribution. The distribution of arrival directions of selected events is presented in Fig.3 by black points along background of sky visibility, i.e.

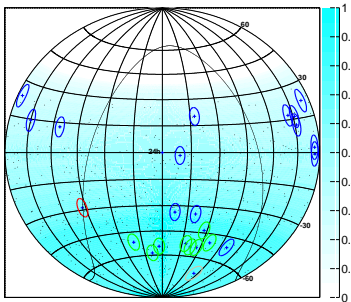


**Fig. 3.** A skymap of time visibility for the Baikal NT200 and data sample in equatorial coordinates with placed 14 classical dSphs (blue circles), 8 new discovered faint dwarfs (yellow), the Galactic Center (red) and the LMC (pink).

the part of time during which the particular direction is observed by NT200, shown by gradient in color. Due to the NT200 location and the selection of neutrino events from the lower hemisphere only, in what follows we consider the sources of dark matter annihilation signal with declinations below  $39^\circ N$ . Full visibility is reached for declinations larger  $39^\circ S$ .

### 3. SIGNAL AND BACKGROUND

In search for neutrino fluxes above the expected background of atmospheric neutrinos, we test 23 directions including those towards a set of dSphs and the LMC on the skymap. In Fig.3 are drawn the coordinates of 14 classical dark dwarf galaxies by blue crosses (and 5 degrees circles around them): "Carina", "Fornax", "Leo-I", "Leo-II", "Sculptor", "Sextans", "Bootes-I", "Coma Berenices", "Hercules", "Leo-IV", "Leo-V", "Leo-T", "Segue-1", "Segue-2". There are also 8 ultra faint dSphs discovered recently by the DES collaboration [8] at declinations larger 45°S. They are marked by yellow 5 degrees circles in Fig.3: "Reticulum-2", "Eridanus-2", "Horologium-1", "Pictor-1", "Phoenix-2", "Indus-1", "Eridanus-3", "Tucana-2". In Table 1 all 22 dwarf galaxies are presented along with their galactic coordinates ( $\delta$ ,  $\alpha$ ).

Name	Dec	RA	$\overline{\log_{10} J}$	$N_S$	$N_B$	TS, $b\bar{b}$ 30 GeV	TS, $\nu\bar{\nu}$ 10 TeV
Carina	-50.97	100.40	$18.1\pm 0.23^a$	30	29.3	0.10	1.11
Fornax	-34.45	40.0	$18.2\pm 0.21^a$	25	26.0	0.02	0
Leo-I	12.31	152.12	$17.7\pm 0.18^a$	14	11.6	1.15	0.05
Leo-II	22.15	168.37	$17.6\pm 0.18^a$	11	6.81	2.19	0
Sculptor	-33.71	15.04	$18.6\pm 0.18^a$	29	24.5	0	0.25
Sextans	-1.61	18.26	$18.4\pm 0.27^a$	23	17.6	2.50	0
Bootes-I	14.50	210.03	$18.8\pm 0.22^a$	12	10.7	0.05	0.95
Coma Berenices	23.90	186.75	$19.0\pm 0.25^a$	10	6.12	0.76	0.12
Hercules	12.79	247.76	$18.1\pm 0.25^a$	9	11.3	0	0
Leo-IV	-0.53	173.24	$17.9\pm 0.28^a$	18	16.8	0.0	0.48
Leo-V	2.22	172.79	$16.37\pm 0.9^b$	18	15.4	0.0	0
Leo-T	17.05	143.72	$17.11\pm 0.4^b$	14	9.34	0	0
Segue-1	16.08	151.77	$19.5\pm 0.29^a$	13	9.76	1.28	0.78
Segue-2	20.18	34.82	$16.21\pm 1.0^b$	8	7.83	0.03	0.99
Reticulum-2	-54.05	53.92	$19.8\pm 0.9^c$	20	28.7	0.01	0.76
Eridanus-2	-43.53	56.09	$17.3\pm 0.4^d$	25	27.5	0	0
Horologium-1	-54.11	43.87	$18.4\pm 0.4^d$	22	28.8	1.02	0
Pictor-1	-50.28	70.95	$18.1\pm 0.4^d$	19	28.6	0	0
Phoenix-2	-54.41	354.99	$18.4\pm 0.4^d$	35	28.2	2.34	0
Indus-1	-51.16	317.20	$18.3\pm 0.4^d$	28	27.3	0	0
Eridanus-3	-52.28	35.69	$18.3\pm 0.4^d$	29	28.7	0.63	4.96
Tucana-2	-58.57	343.06	$18.8\pm 0.4^d$	31	27.4	2.38	1.98

**Table 1.** List of dwarf galaxies used in the present analyses, their coordinates and  $J_a$ -factors integrated over 20° opening angle, number of observed events  $n$  and expected number of background events  $N_B$  in the signal region, test statistics (TS) for supposed signal with  $m_{DM} = 30$  GeV and  $b\bar{b}$  channel and with  $m_{DM} = 10$  TeV and  $\nu\bar{\nu}$  channel. Uncertainties in the  $J_a$ -factors are marked with superscripts corresponding to the following references:

*a)* [37], *b)* [38], *c)* [39], *d)* [14].

Neutrino flux from dark matter annihilations in a galaxy in direction at an angle  $\psi$  with respect to its center is given by

$$\frac{d\phi_\nu}{dE_\nu d\Omega} = J_a(\psi) \frac{\langle\sigma_a v\rangle}{8\pi m_{DM}^2} \frac{dN_\nu}{dE_\nu}. \quad (1)$$

Part of this expression depends on particle physics properties of dark matter:  $\langle\sigma_a v\rangle$  is its annihilation cross section in present time,  $dN_\nu/dE_\nu$  is energy spectrum of neutrinos generated in decays processes of products

of DM annihilations in dependence on masses of dark matter particles  $m_{DM}$ . In what follows we consider the DM mass interval from 30 GeV to 10 TeV. Neutrino energy spectra depend on properties of dark matter annihilation. We consider a set of five benchmark annihilation channels:  $b\bar{b}$ ,  $\tau^+\tau^-$ ,  $\mu^+\mu^-$ ,  $W^+W^-$  and  $\nu\bar{\nu} \equiv \frac{1}{3}(\nu_e\bar{\nu}_e + \nu_\mu\bar{\nu}_\mu + \nu_\tau\bar{\nu}_\tau)$ . For the present analysis the neutrino energy spectra in these channels have been taken from Ref. [35]. Due to the loss of coherence after propagation over cosmologically large distances neutrino arrive at the Earth as mass states and to calculate  $\nu_\mu$  ( $\bar{\nu}_\mu$ ) energy spectra we use the following set [36] of neutrino oscillation parameters:  $\Delta m_{21}^2 = 7.6 \cdot 10^{-5} \text{ eV}^2$ ,  $\Delta m_{31}^2 = 2.48 \cdot 10^{-3} \text{ eV}^2$ ,  $\delta_{CP} = 0$ ,  $\sin^2 \theta_{12} = 0.323$ ,  $\sin^2 \theta_{23} = 0.567$ ,  $\sin^2 \theta_{13} = 0.0234$ .

Astrophysical part of the neutrino flux (1) is encoded in the values of  $J_a$ -factors which depend on the dark matter content and angular distance between direction of observation and the direction towards the center of the corresponding source. This quantity is given by the following integral over line-of-sight

$$J_a(\psi) = \int_0^{l^{max}} dl \rho^2 \left( \sqrt{R_0^2 - 2lR_0 \cos \psi + l^2} \right) \quad (2)$$

of dark matter density  $\rho(r)$  squared. In eq. (2),  $R_0$  is the distance from the center of the source to the Solar System. The larger value of annihilation factor  $J_a(\psi)$ , the larger magnitude of the neutrino flux is expected at the Earth. Total expected number of signal events to be detected by neutrino telescope NT200 from dark matter annihilations in a distant source can be calculated using eq. (1) as follows

$$N_S = T \frac{\langle \sigma_a v \rangle}{8\pi m_{DM}} J_{\Delta\Omega} \int_{E_{th}}^{m_{DM}} dE_\nu \frac{dN_\nu}{dE_\nu} S_\nu(E_\nu). \quad (3)$$

Here  $T$  is the livetime,  $S_\nu(E_\nu)$  is the effective area of the telescope for neutrinos coming from the direction towards the source in quest and

$$J_{\Delta\Omega} = \int d(\cos \psi) d\phi J(\psi), \quad (4)$$

where the integral is taken over a search region to be discussed below. The effective area  $S_\nu(E_\nu)$  is calculated from MC simulations (see section 1) by determination of detection efficiency of muon neutrino coming from a particular direction. We refer reader to Refs. [28, 29] for detailed discussions.

In the following analysis we consider the distant dwarfs galaxies as point like sources since their angular sizes are well within angular resolution of the NT200. In Table 1 we present the values of  $J$ -factor (4) for these galaxies integrated over solid angle corresponding to their sizes. Also we include the astrophysical uncertainties in the estimates of  $J$ -factors with corresponding references. In the chosen set of dwarf galaxies the largest  $J_a$ -factor is expected from ‘‘Reticulum-2’’. As it has been discussed in Ref. [39], this source is a very attractive target in search for DM signal.

Great interest to test direction towards the LMC is motivated by recent dark matter analysis of FERMI-LAT data performed in [22] indicating the LMC to be the next after the GC bright source of the annihilation signal. Position of this source on the sky allows for 100% time observation in neutrinos by NT200. In performance of the DM signal from the LMC we take into account extended size of this galaxy and simulate neutrino signal using dark matter density profile [40–42] of the following functional form

$$\rho(r) = \frac{\rho_0}{\left(\frac{r}{r_S}\right)^\gamma \left[1 + \left(\frac{r}{r_S}\right)^\alpha\right]^{\frac{\beta-\gamma}{\alpha}}} \theta(r_{max} - r).$$

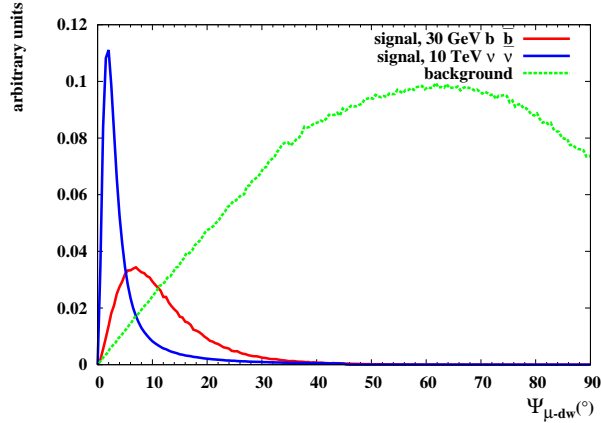


Fig. 4. Angular distributions of signal ( $b\bar{b}$ ,  $m_{DM} = 30$  GeV and  $\nu\bar{\nu}$ ,  $m_{DM} = 10$  TeV) and background events for “Reticulum-2” as a source.

Here  $r_{max} = 100$  kpc,  $\theta(r)$  is the step function. Following Ref. [22] we consider three dark matter halo profiles to be referred as *sim-mean*, *sim-min* and *sim-max*. Corresponding parameters  $\alpha$ ,  $\beta$ ,  $\gamma$  and  $r_S$  are presented in Table 2. We used *sim-mean* profile to obtain the upper limits and the others, i.e. *sim-min* and *sim-max*, to

Profile	$\alpha$	$\beta$	$\gamma$	$r_S$ , kpc	$\rho_0$ , GeV/cm <sup>3</sup>	$\overline{\log_{10} \mathcal{J}}$
<i>sim-max</i>	0.35	3.0	1.3	5.4	4.19	21.94
<i>sim-mean</i>	0.96	2.85	1.05	7.2	0.32	20.38
<i>sim-min</i>	1.56	2.69	0.79	4.9	0.46	20.25

Table 2. Parameters of dark matter halo profiles for Large Magellanic Cloud [22].

estimate the influence of astrophysical systematic uncertainties. We note that there is also an uncertainty in determination of the gravitational center of the LMC. Its size is within about  $1.5^\circ$  [22] which is considerably smaller than the angular resolution of NT200. In the present analysis we choose the coordinates of the LMC center  $l = 280.54^\circ$ ,  $b = -32.51^\circ$  derived from stellar rotation curves [43]. We see that  $J_a$ -factor of LMC integrated over search region is larger than that of all dwarfs (see Tables 1 and 2) which along with 100% visibility makes this source very attractive for searches for dark matter signal.

We simulate the expected energy and angular distribution of the signal events from dwarf galaxies and LMC as described in Ref. [29]. Atmospheric neutrinos are dominating source of the background. In the present analysis we estimate the expected background from the data using scrambling by randomization of RAs of the observed events. This procedure can not exclude a possible signal contamination in our determination of the background which is however expected to be small. In Fig. 4 we present comparison of angular distribution of signal and background for “Reticulum-2” for an example. Here we show angular distributions of the signal for the softest ( $b\bar{b}$ ,  $m_{DM} = 30$  GeV) and hardest ( $\nu\bar{\nu}$ ,  $m_{DM} = 10$  TeV) among the chosen annihilation channels. We see that the angular spread of the signal varies up to  $20 - 25^\circ$ ; the most collimated signal is produced in monochromatic neutrino channel.



## 4. DATA ANALYSIS

The analysis is performed by construction of likelihood function along the same lines as described in Ref. [29]. For obtained angular spreads of signal events from the sources we choose as search region a cone with half-cone angle of  $20^\circ$  around each single source. The numbers of observed and background events within this cone for each probing direction towards corresponding dwarf galaxy are presented in Table 1. In the search region of the LMC the number of observed events is 23 and the expected background is estimated as 29.5.

Given the expected angular signal and background distributions for a source,  $f_S(\psi)$  and  $f_B(\psi)$ , respectively, the resulting angular distribution has the form

$$f(\psi, N_S, N_B) = \frac{1}{N_S + N_B} (N_S f_S(\psi) + N_B f_B(\psi)), \quad (5)$$

where  $N_S$  and  $N_B$  are expected number of signal and background events inside the search region, respectively. The likelihood function for a particular source can be written as follows

$$\mathcal{L}(\langle \sigma_a v \rangle) = \frac{(N_B + N_S)^n}{n!} e^{-(N_B + N_S)} \times \prod_{i=1}^n f(\psi_i, N_B, N_S), \quad (6)$$

where  $n$  is the observed number of events and the first multiplier accounts for statistical fluctuations in  $n$ . To take into account systematic uncertainties the likelihood function is modified by introducing a set of nuisance parameters  $\theta = \{\epsilon_S, \epsilon_B, J\}$  which change (6) as

$$\mathcal{L}(\langle \sigma_a v \rangle, \theta) = \mathcal{N} \frac{(\epsilon_B N_B + \epsilon_S N_S)^n}{n!} e^{-(\epsilon_B N_B + \epsilon_S N_S) - \frac{(\epsilon_S - 1)^2}{2\sigma_S^2} - \frac{(\epsilon_B - 1)^2}{2\sigma_B^2} - \frac{(\log_{10}(J) - \overline{\log_{10}(J)})^2}{2\sigma_J^2}} \prod_{i=1}^n f(\psi_i, \epsilon_B N_B, \epsilon_S N_S). \quad (7)$$

Here the dependence on  $\langle \sigma_a v \rangle$  and  $J$  enters implicitly through  $N_S$  via Eq. (3). In the above expression  $\sigma_S$  and  $\sigma_J$  are particle physics and astrophysical systematic in the signal, while  $\sigma_B$  is the systematic uncertainty in the background. We intentionally divide systematic uncertainties in number of signal events coming from particle physics and from astrophysics. The latter enters into the likelihood function through estimates of error in  $J_a$ -factors presented in Table 1. For careful discussion of other sources of systematic uncertainties we refer reader to Refs. [28, 29]. Their size is dominated by 30% experimental uncertainty resulting from optical properties of water and in the sensitivity of the optical modules. Theoretical errors reach 10-12% coming from uncertainties in neutrino oscillation parameters and neutrino-nucleus interaction cross section.

The upper limits on  $\langle \sigma_a v \rangle$  are then obtained using profile likelihood constructed as

$$\lambda(\langle \sigma_a v \rangle) = -2 \ln \frac{\mathcal{L}(\langle \sigma_a v \rangle, \hat{\theta}(\langle \sigma_a v \rangle))}{\mathcal{L}(\widehat{\langle \sigma_a v \rangle}, \hat{\theta})}. \quad (8)$$

Here  $\widehat{\langle \sigma_a v \rangle}$  and  $\hat{\theta}$  are the values which give absolute maximum to the likelihood probability function in physical region with  $\langle \sigma_a v \rangle \geq 0$ , while  $\hat{\theta}(\langle \sigma_a v \rangle)$  denotes the value of the nuisance parameters  $\theta$  in the maximum of the likelihood at fixed value of  $\langle \sigma_a v \rangle$ . For analysis with the LMC we do not include astrophysical systematic in the likelihood function but instead we calculate upper limits for different dark matter density profiles *sim-min* and *sim-max* considering them as limiting cases (see discussion of sources of astrophysical uncertainties in [22]). In the joint analysis with several dwarf galaxies corresponding likelihood function is constructed as a product of



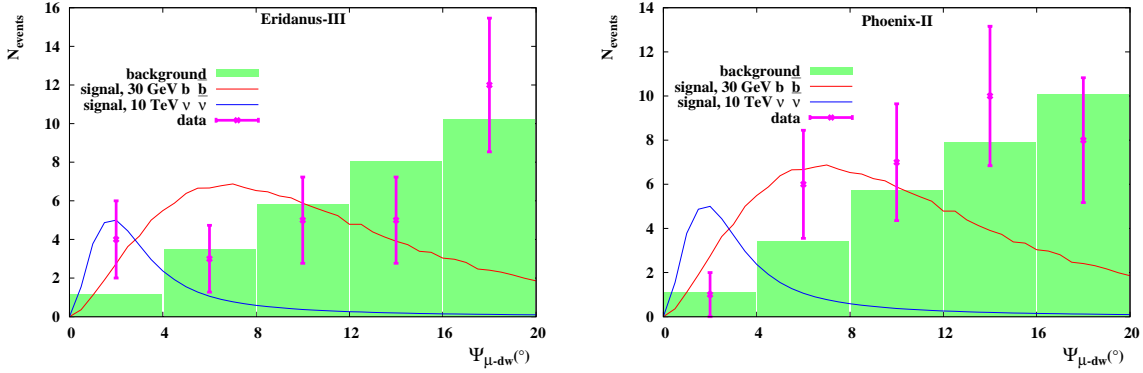


**Fig. 5.** Angular distributions of signal ( $b\bar{b}$ ,  $m_{DM} = 30$  GeV and  $\nu\bar{\nu}$ ,  $m_{DM} = 10$  TeV) in comparison with the data and background events “Eridanus-3” (left) and “Phoenix-2” (right).

individual likelihood functions as follows

$$\mathcal{L}(\langle\sigma_a v\rangle, \theta) = \prod_{i=1}^{N_d} \mathcal{L}_i(\langle\sigma_a v\rangle, \theta_i). \quad (9)$$

Here  $N_d$  is the number of sources taken in the joint analysis and  $\mathcal{L}_i(\langle\sigma_a v\rangle, \theta_i)$  is the individual likelihood function of  $i$ -th source.

We start our consideration with the chosen set of dwarf spheroidal galaxies. Firstly, we look for an excess of events in the direction of each individual source in the search region neglecting presence of other sources of dark matter annihilations. We do not find any excess in the directions towards any of 22 chosen dwarf spheroidals as compared to the expected background. To quantify potential deviations from the background only hypothesis we calculate test statistics (TS) which is defined as  $\lambda(0)$ , see eq. (8). Values of TS for two benchmark annihilation channels  $\nu\bar{\nu}$  with  $m_{DM} = 10$  TeV and  $b\bar{b}$  with  $m_{DM} = 30$  GeV are presented in Table 1. These channels have the most and less narrow angular distribution, respectively. Difference in the forms of these distributions results in distinction in the values of TS. Maximal deviation from the background only hypothesis has been observed for “Eridanus-3” source; the largest TSs reach values about 5 for large mass region which correspond to more collimated signal distributions. In Fig. 5 we present distribution of observed events in comparison with the background and signal distribution for two selected sources, “Eridanus-3” (left) and “Phoenix-2” (right). In the former case we observe an excess of events at small angles with respect to the source which resulted in an increase of TS for channels with large masses of dark matter particles. In the case of “Phoenix-2”, the data prefer more wide signal angular distribution because there is an increase of events at moderate values of  $\psi$ , in the region  $5 - 15^\circ$ . For the case of the LMC the test statistics appears to be zero for all chosen annihilation channels due to found deficit in observed events as compared to background.

For the following part of the analysis out of the whole set we select 5 dwarf spheroidals, such that they have the largest values of  $J_a$ -factors and good visibility on the one hand and expected signal regions for every galaxy in this set do not intersect with each other. The selected set contains “Sculptor”, “Coma Berenices”, “Segue-1”, “Reticulum-2”, “Tucana-2”. This choice allows us not only to obtain the individual upper limits on annihilation cross section but also to find the upper limits from combination of observations of several independent sources<sup>1)</sup>.

<sup>1)</sup> The case when the galaxies have small angular distance is more involved and requires additional simulation of signal angular distribution.

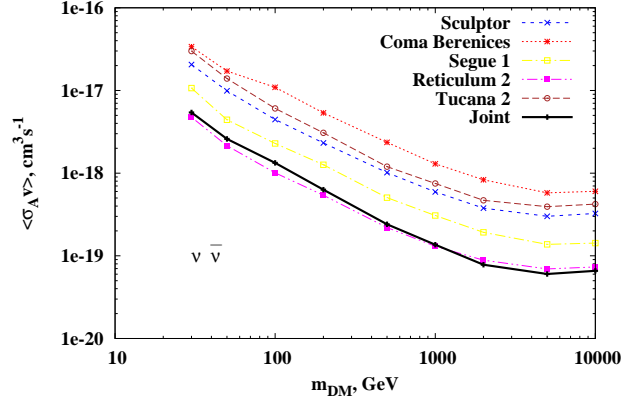


Fig. 6. 90% CL upper limits from the NT200 data on dark matter annihilation cross section assuming annihilation to  $\nu\bar{\nu}$  for selected set of dwarf spheroidal galaxies and from their combination.

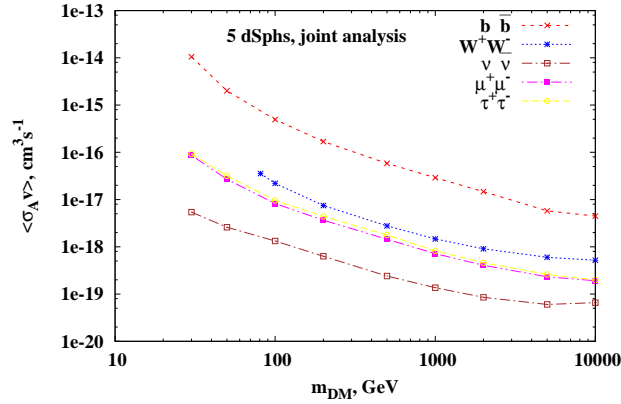


Fig. 7. 90% CL upper limits from the NT200 data on dark matter annihilation cross section assuming annihilation to  $b\bar{b}$ ,  $W^+W^-$ ,  $\mu^+\mu^-$ ,  $\tau^+\tau^-$  and  $\nu\bar{\nu}$  from joint analysis of dwarf spheroidals.

The individual and joint 90% upper limits on  $\langle\sigma_a v\rangle$  are obtained by using Feldman-Cousins approach [44]. In Fig. 6 we show the upper limits for 5 chosen dwarfs and the results of combined analysis (marked as *Joint*) for  $\nu\bar{\nu}$  annihilation channel. The strongest individual upper limit comes from observation of “Reticulum-2” direction. It is determined by the largest annihilation  $J_a$ -factor and the position of this source on the sky which allows for 100% visibility from the NT200 position. Although “Segue-1” has similar value of  $J$ -factor with smaller astrophysical uncertainty than those of Reticulum-2, this source is visible only about 32% of the whole lifetime. The limits from directions towards “Sculptor”, “Coma Berenices” and “Tucana-2” are even weaker. The result of combined analysis is determined mainly by the strongest bound from “Reticulum-2”. Similar picture is obtained for other annihilation channels. We compare the upper limits from combined analysis of dwarfs from different channels in Fig. 7. The strongest upper limit on annihilation cross section from this search reach values about  $6 \cdot 10^{-20} \text{ cm}^3/\text{s}$  for monochromatic neutrino annihilation channel. Flattening of the results for all channels (especially for  $\nu\bar{\nu}$ ) for very large masses of dark matter particles comes from softer neutrino energy spectrum which results from enhancement due to electroweak corrections [45].

Next, we consider Large Magellanic Cloud as the source of products of dark matter annihilations. As we discussed above we use *sim-mean* profile as a default for the LMC and the profiles marked *sim-min* and *sim-max*

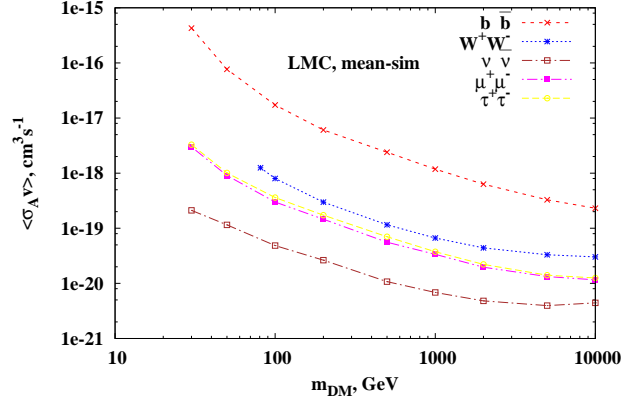


Fig. 8. 90% CL upper limits from the NT200 data on dark matter annihilation cross section assuming annihilation to  $b\bar{b}$ ,  $W^+W^-$ ,  $\mu^+\mu^-$ ,  $\tau^+\tau^-$  and  $\nu\bar{\nu}$  from analysis of the LMC direction.

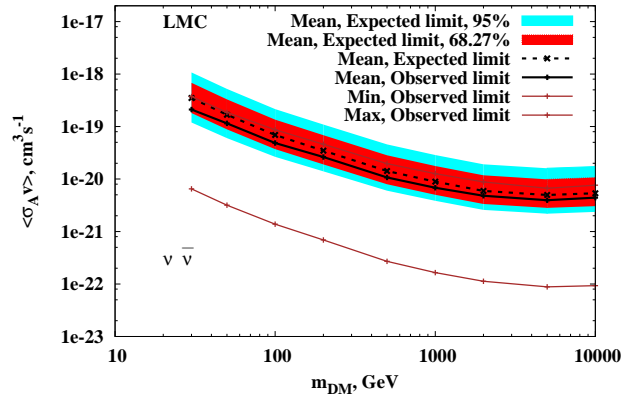


Fig. 9. 90% CL upper limits from the NT200 data assuming different dark matter density profiles for LMC (solid lines) and sensitivity (dashed line) on dark matter annihilation cross section assuming annihilation to  $\nu\bar{\nu}$ . Colored bands represent 68% (red) and 95% (blue) quantiles.

to estimate astrophysical uncertainty. In Fig. 8 we show 90% CL upper limits on dark matter annihilation cross section for different annihilation channels. The most stringent bounds are obtained for  $\nu\bar{\nu}$  and reach values about  $7 \cdot 10^{-21} \text{cm}^3/\text{s}$ .

Using estimated background we run a set of pseudoexperiments to find the sensitivity of the NT200 to the neutrino signal from dark matter annihilations in the LMC. We show this sensitivity for  $\nu\bar{\nu}$  annihilation channel in Fig. 9 (at 1- and 2- $\sigma$  level) along with 68% (red) and 95% (blue) quantiles in comparison with the obtained 90% CL upper limit shown by the black solid line assuming *sim-mean* profile. Also in this Figure we show 90% CL upper limits for this annihilation channel obtained with the other dark matter density profiles, *sim-min* and *sim-max*, which can be viewed as an estimate of astrophysical systematics related to this source. We see that with “cuspy” *sim-max* profile the upper bounds are improved by almost two orders of magnitude.

In Fig. 10 we present a comparison of upper limits obtained by different neutrino experiments from their searches for the dark matter annihilation signal in comparison with the NT200 results. There are shown the limits from IceCube (GC [46] and preliminary results from joint analysis of dwarf galaxies [18]), ANTARES (GC [47]), Super-Kamiokande (GC [48]) as well as NT200 limit from the analysis of GC [29]. In Fig. 11 we

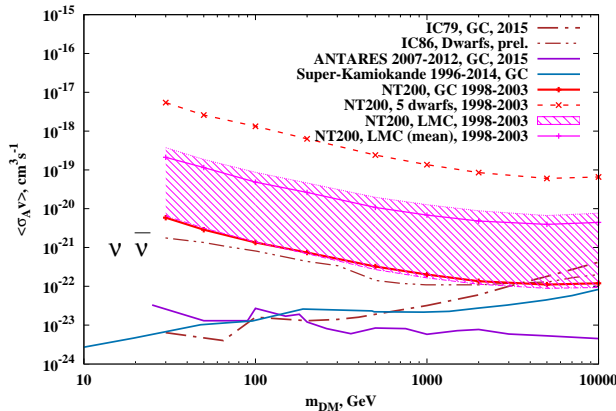


Fig. 10. 90% CL upper limits on dark matter annihilation cross section assuming annihilation to  $\nu\bar{\nu}$  obtained with the NT200 dataset (magenta line and shaded area) in this study and in the GC (red line) analysis [29] in comparison with results from ANTARES [47], IceCube [46] and Super-Kamiokande [48].

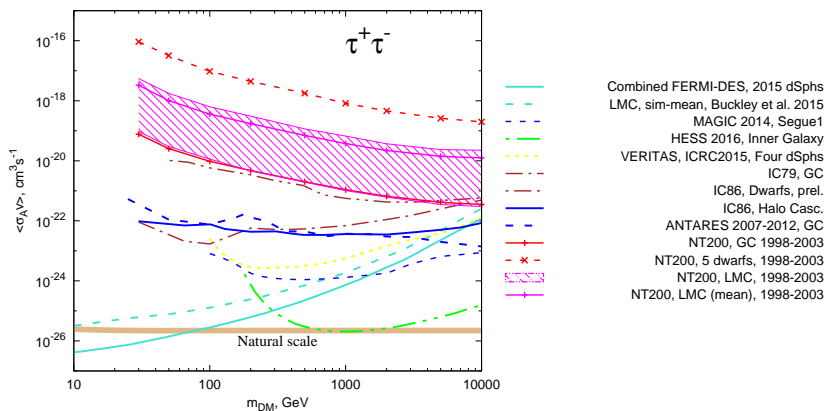


Fig. 11. 90% CL upper limits on dark matter annihilation cross section assuming annihilation to  $\tau^+\tau^-$  in comparison with other experiments.

compare the 90% CL upper limits on annihilation cross section for  $\tau^+\tau^-$  annihilation channel obtained by different experiments. These experiments include the FERMI [14] (dwarf galaxies, DES), VERITAS [49] (four dwarf galaxies), MAGIC [16] (Segue 1), HESS [17] (inner Galactic halo), IceCube (Milky Way [50], GC [46] and preliminary results for dwarf galaxies [18]), ANTARES [47] (GC). Light brown line shows the thermal relic annihilation cross section from Ref. [51]. From the present analysis we see that for Baikal experiment the LMC direction is more sensitive (even with astrophysical systematics) to dark matter annihilation signal as compared to that of dwarf spheroidal galaxies.

### 5. CONCLUSIONS

To summarize, we presented our new results in indirect search for dark matter signal from distant astrophysical sources, namely the Large Magellanic Cloud and dwarfs spheroidal galaxies, with neutrino events of the NT200 neutrino telescope in Lake Baikal. No significant excess in these directions has been found. We obtained the upper limits at 90% CL on annihilation cross sections for different annihilation channels and masses of dark

matter particles in the range from 30 GeV to 10 TeV. In the present study, the strongest bound on dark matter annihilation cross section has been found is about  $6 \cdot 10^{-20} \text{ cm}^3/\text{s}$  for combination of results from dwarfs and about  $7 \cdot 10^{-21} \text{ cm}^3/\text{s}$  for the LMC. We expect considerable improvement of these results with data coming from Baikal-GVD experiment [52].

The work of S.V. Demidov and O.V. Suvorova was supported by the RSCF grant 14-12-01430.

## REFERENCES

1. G. Bertone, D. Hooper and J. Silk, Phys. Rept. **405** 279 (2005). [hep-ph/0404175].
2. G. Steigman and M. S. Turner, Nucl. Phys. B **253** 375 (1985).
3. L. E. Strigari, J. S. Bullock, M. Kaplinghat, J. D. Simon, M. Geha, B. Willman and M. G. Walker, Nature **454**, 1096 (2008); arXiv:0808.3772.
4. Y. Yang, F. Hammer, S. Fouquet, H. Flores, M. Puech, M. S. Pawlowski, P. Kroupa, Mon.Not.Roy.Astron.Soc. **442** no.3, 2419-2433 (2014); arXiv:1405.2071.
5. P. Colin, A. Klypin, O. Valenzuela, S. Gottlober, APJ, **612**:50-57 (2004).
6. A. V. Kravtsov, Adv.Astron. **2010** 281913 (2010).
7. A. Rodriguez-Puebla, P. Behroozi, J. Primack, A. Klypin, Ch. Lee, D. Hellinger, Mon.Not.Roy.Astron.Soc. **462** no.1, 893-916 (2016); arXiv:1602.04813.
8. K. Bechtol *et al.* [DES Collaboration], Astrophys. J. **807** no.1, 50, (2015); arXiv:1503.02584.
9. A. Drlica-Wagner *et al.* [DES Collaboration], Astrophys. J. **813** no.2, 109 (2015); arXiv:1508.03622.
10. T. Abbott *et al.* [Dark Energy Survey Collaboration], (2005), arXiv:0510346; <https://www.darkenergysurvey.org/news-and-results/publications>.
11. P. A. Abell *et al.*, [LSST Science Collaborations], (2009), arXiv:0912.0201; <https://www.lsst.org/scientists/scibook>.
12. M. Doro *et al.* [CTA Consortium Collaboration], Astropart.Phys. **43** 189 (2013); arXiv:1208.5356.
13. M. Ackermann *et al.* [Fermi-LAT Collaboration], Phys. Rev. Lett. **115** no.23, 231301 (2015); arXiv:1503.02641.
14. A. Drlica-Wagner *et al.* [Fermi-LAT and DES Collaborations], Astrophys. J. **809** no.1, L4 (2015); arXiv:1503.02632.
15. A. Albert *et al.* [Fermi-LAT and DES Collaborations], (2016); arXiv:1611.03184.
16. J. Aleksic *et al.*, JCAP **1402** 008 (2014); arXiv:1312.1535.
17. H. Abdallah *et al.* [HESS Collaboration], Phys. Rev. Lett. **117** no.11, 111301 (2016); arXiv:1607.08142.
18. M. G. Aartsen *et al.* [IceCube Collaboration], (2015); arXiv:1510.05226.
19. A. Tasitsiomi, J. M. Siegal-Gaskins, and A. V. Olinto, Astropart.Phys. **21**, 637 (2004); arXiv:0307.375.

20. K. N. Abazajian and M. Kaplinghat, Phys.Rev. D86 083511 (2012); arXiv:1207.6047.
21. (2015); arXiv:1511.02938.
22. M. R. Buckley, E. Charles, J. M. Gaskins, A. M. Brooks, A. Drlica-Wagner, P. Martin and G. Zhao, Phys. Rev. D **91** no.10, 102001 (2015); arXiv:1502.01020.
23. Zh.-A.M. Dzhilkibaev, G.V. Domogatsky, O.V. Suvorova, Phys.Usp. 58 no.5, 495-502 (2015).
24. I.A. Belolaptikov et al., [Baikal Collab.], Astropart.Phys. 7, 263-282 (1997).
25. V.M. Aynutdinov et al., [Baikal Collab.], Phys.Atom.Nucl. 69, 1914-1921 (2006).
26. V. Aynutdinov et al., [Baikal Collab.], Izvestia Akademii Nauk (Izvestia Russ. Academy Science), Ser. Phys., vol. 71, N. 4, (2007).
27. V. Aynutdinov et al., [Baikal Collab.], Nucl. Instrum. Methods, vol A602, p 14, (2009).
28. A. D. Avrorin *et al.*, [Baikal Collaboration], Astropart. Phys. **62** 12 (2014); arXiv:1405.3551.
29. A. D. Avrorin *et al.*, [Baikal Collaboration], Astropart.Phys. 81, 12-20 (2016); arXiv:1512.01198.
30. A.V. Avrorin et al., [Baikal Collab.], Phys.Part.Nucl.Lett. 8, 704-716 (2011).
31. I. A. Belolaptikov, Preprint of INR RAS 1178/2007 (in Russian), (2007).
32. D. Heck *et al.*, Forschungszentrum Karlsruhe, Technical Report No. 6019, (1998).
33. E. Bugaev, S. Klimushin, I. Sokalsky, Phys. Rev. D, vol. 64, p. 074015, (2001).
34. V. Agrawal, T. Gaisser, P. Lipari and T. Stanev, Phys. Rev., vol. D53, p. 1314, (1996).
35. P. Baratella, M. Cirelli, A. Hektor, J. Pata, M. Piibeleht and A. Strumia, (2013); arXiv:1312.6408.
36. D. V. Forero, M. Tortola and J. W. F. Valle, Phys. Rev. D **90** 093006, (2014); arXiv:1405.7540.
37. M. Ackermann *et al.* [Fermi-LAT Collaboration], Phys. Rev. D **89**, 042001 (2014); arXiv:1310.0828.
38. A. Geringer-Sameth, S. M. Koushiappas and M. Walker, Astrophys. J. **801** no.2, 74, (2015); arXiv:1408.0002.
39. V. Bonnivard *et al.*, Astrophys. J. **808** no.2, L36, (2015); arXiv:1504.03309.
40. L. Hernquist, Astrophys. J. **356**, 359 (1990).
41. H. Zhao, Mon. Not. Roy. Astron. Soc. **278**, 488 (1996); arXiv:9509.122.
42. A. V. Kravtsov, A. A. Klypin, J. S. Bullock and J. R. Primack, Astrophys. J. **502** 48, (1998); arXiv:9708.176.
43. R. P. van der Marel, D. R. Alves, E. Hardy and N. B. Suntzeff, Astron. J. **124** 2639, (2002); arXiv:0205.161.
44. G. J. Feldman and R. D. Cousins, Phys. Rev. D **57** 3873, (1998); arXiv:9711.021.
45. M. Cirelli *et al.*, JCAP **1103** 051, (2011), Erratum: [JCAP **1210** (2012) E01]; arXiv:1012.4515.
46. M. G. Aartsen *et al.*, [IceCube Collaboration], Eur. Phys. J. C **75** 10, 492, (2015); arXiv:1505.07259.

47. S. Adrian-Martinez *et al.* [ANTARES Collaboration], JCAP **1510** 10, 068, (2015); arXiv:1505.04866.
48. K. Frankiewicz [Super-Kamiokande Collaboration], (2015); arXiv:1510.07999.
49. B. Zitzer [VERITAS Collaboration], (2015); arXiv:1509.01105.
50. M. G. Aartsen *et al.* [IceCube Collaboration], Eur. Phys. J. C **76** no.10, 531, (2016); arXiv:1606.00209.
51. G. Steigman, B. Dasgupta and J. F. Beacom, Phys. Rev. D **86** 023506, (2012); arXiv:1204.3622.
52. A. D. Avrorin *et al.*, PoS EPS -**HEP2015** 418, (2015); arXiv:1511.02324.